# POLITECNICO DI TORINO Repository ISTITUZIONALE

Off-axis damage tolerance of fiber-reinforced composites for aerospace systems

#### Original

Off-axis damage tolerance of fiber-reinforced composites for aerospace systems / Galizia, P.; Sciti, D.; Saraga, F.; Zoli, L.. - In: JOURNAL OF THE EUROPEAN CERAMIC SOCIETY. - ISSN 0955-2219. - STAMPA. - 40:7(2020), pp. 2691-2698. [10.1016/j.jeurceramsoc.2019.12.038]

Availability:

This version is available at: 11583/2952101 since: 2022-01-21T14:12:21Z

Publisher: Elsevier Ltd

Published

DOI:10.1016/j.jeurceramsoc.2019.12.038

Terms of use:

This article is made available under terms and conditions as specified in the corresponding bibliographic description in the repository

Publisher copyright

Elsevier postprint/Author's Accepted Manuscript

© 2020. This manuscript version is made available under the CC-BY-NC-ND 4.0 license http://creativecommons.org/licenses/by-nc-nd/4.0/.The final authenticated version is available online at: http://dx.doi.org/10.1016/j.jeurceramsoc.2019.12.038

(Article begins on next page)

Off-axis damage tolerance of fiber-reinforced composites for aerospace

systems

P. Galizia\*, D. Sciti, F. Saraga and L. Zoli

CNR-ISTEC, National Research Council of Italy - Institute of Science and Technology for

Ceramics, Via Granarolo 64, Faenza, Italy-48018

Abstract

Off-axis strength retention of continuous carbon fiber-reinforced dense ZrB<sub>2</sub>-based ceramics

(C<sub>f</sub>/ZrB<sub>2</sub>) after thermal or indentation damage was evaluated. Thermal damage was in-situ

induced and characterized by cyclic dilatometric analysis. Indentation damage was induced

through Vickers indentation and then characterized by digital microscopy. The investigation of

Vickers imprints suggested that residual stresses promoted the material pileup onto the fibers'

plane and the appearance of out-of-plane freed fibers (OFF). On the other hand, thermal

damage reduced the residual stresses and left inner freed fibers (IFF) that enhanced the elastic

response. Finally, the flexural tests on damaged specimens unexpectedly revealed that C<sub>f</sub>/ZrB<sub>2</sub>

kept its load bearing capability either after thermal or indentation damage (in both cases) and

showed damage insensitivity although tested in fully matrix-dominated loading configuration

(off-axis configuration).

**Keywords**: transverse direction; anisotropic porous ZrB<sub>2</sub>; continuous fiber ceramic composites

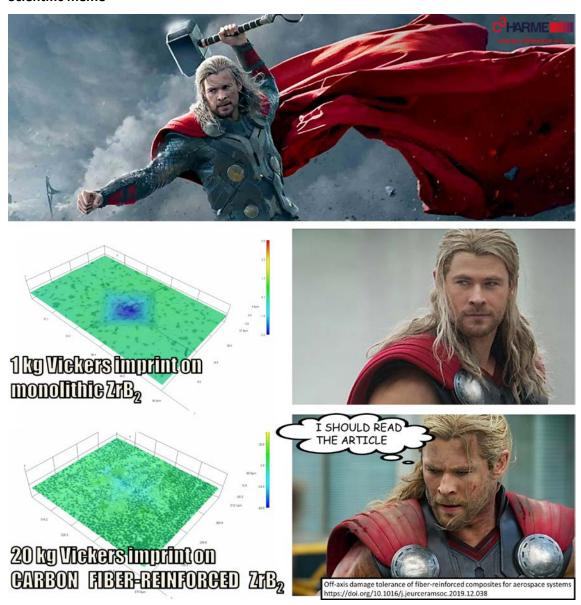
(CFCC); Vickers indentation; pile-up.

https://doi.org/10.1016/j.jeurceramsoc.2019.12.038

\*corresponding author, e-mail: pietro.galizia@istec.cnr.it

1

# Scientific meme



<sup>\*</sup>corresponding author, e-mail: pietro.galizia@istec.cnr.it

#### 1. Introduction

Ultra-high temperature ceramic matrix composites (UHTCMCs) are currently attracting increasing research interest for their potential impact in the aerospace field [1,2]. With respect to the already used C/SiC composites for nose cones, leading edges and rocket nozzles, UHTCMCs promise to increase the operating limit from ~1600°C to above 2000°C while keeping good structural behaviour, dimensional tolerances and thermal shock resistance [1,3]. UHTCMCs are based on a dense-matrix of borides, carbides or nitrides such as ZrB2, HfB2, ZrC, HfC, TaC, HfN, and carbon fiber reinforcement (Cf). The former is characterized by high melting points, high hardness, chemical inertness and relatively good resistance to oxidation in severe environments [4-7]. The latter should enhance the damage tolerance and thermal shock resistance [8]. Since 2015, the properties of the "baseline UHTCMC" based on ZrB2 matrix reinforced with unidirectional 45 vol% of high-modulus carbon fiber have been greatly improved, and are showing a considerable margin for further development in terms of structural properties, oxidation and ablation resistance [9-12]. Indeed, the flexural strength reached 360 MPa at RT and 550 MPa at 1500°C, and the fracture toughness 11 MPa·m<sup>1/2</sup> [1,13], compared to the preliminary values of these composite series, e.g. 120 MPa and 8 MPa·m<sup>1/2</sup> for strength and toughness at RT [14]. The composites science agrees that flawtolerant ceramic-matrix composites can be developed by deliberately inducing delamination modes (i.e. H-crack formation). Basically, flaw-tolerant behaviour is promoted by porous matrices (i.e. weak matrix composites, WMCs), or by weak matrix/fiber interfaces (i.e. weak interface composites, WICs) [15,16]. A porosity higher than 10 % could jeopardize ablation, erosion and oxidation resistance, and off-axis strength. On the other hand, it is not easy to obtain WICs with dense-UHTC matrix. A good strategy to achieve weak interfaces is grouping the fibers into bundles in order to exploit the weak  $C_f/C_f$  and  $C_f/ZrB_2$  interfaces within the bundles [13]. Anyway, this architecture, also called "salami-inspired" or "non-periodic", reduces the off-axis strength and is suspected to decrease ablation and oxidation resistance with respect to the corresponding periodic structures [9].

In this work, we showed that sintered UHTC matrix, with just 7 % of residual porosity and reinforced with strongly bonded continuous fibers, was unaffected by thermal damage or indentation. Hence, it is possible to maximize the off-axis strength without compromising the

<sup>\*</sup>corresponding author, e-mail: pietro.galizia@istec.cnr.it

damage-tolerant characteristic as consequence of the "excessive" sintering and strong matrix/fiber interfaces. The supporting results were based on (i) the investigation of the thermal and indentation damage by dilatometric analysis and optical investigation of the indentation imprints, respectively, both along transverse direction (TD) and longitudinal direction (LD); (ii) off-axis strength retention after damage induced by thermal cycling or indentation. Since in the TD the reinforcement effect of the fiber is full, this configuration ensured a valid failure under tensile stress without any interlaminar shear incoming during the bending test. By suppressing the delamination mode, it was guaranteed that the observed flaw-tolerance did not depend on the applied stress and was not deliberately induced [15]. Furthermore, since fibers were perpendicular to the applied tensile stress, they were not the reason of the damage insensitivity as generally observed in CMCs where fibres in the damage zone are subjected to stresses that are comparable in magnitude to the remote stresses [17-19].

#### 2. Materials and methods

# 2.1. Material manufacturing and microstructure characterization

UHTCMCs based on carbon fiber-reinforced  $ZrB_2$  were produced by hot pressing. The pellet, placed in the hot pressing, was pre-compacted with the graphite rams and heated to 900°C at  $15^{\circ}$ C min<sup>-1</sup>. From this temperature a load of 20 MPa was applied and the heating rate was increased at  $45^{\circ}$ C min<sup>-1</sup>. The applied load was increased to 30 MPa when temperature achieved  $1700^{\circ}$ C, and it was held up at 40 MPa to the maximum temperature of  $1900^{\circ}$ C. The maximum temperature was dwelt as long as no further shrinkage was observed (about 10 min). Free cooling followed. The final microstructure consists in 55 vol% of matrix (84 %  $ZrB_2$  + 9 vol% SiC + 7 % pores) and 45 vol% C<sub>f</sub>. Further details on slurry preparation, infiltration, densification, and microstructural and mechanical features of the produced samples were reported in a previously published work [1].

The microstructure was analyzed on polished and fractured surfaces by field emission scanning electron microscopy (FE-SEM, Carl Zeiss  $\Sigma$ IGMA NTS Gmbh Öberkochen, Germany). Bars for thermal and mechanical characterization were machined both in the longitudinal and transverse direction, here forth indicated as AP-ZrB<sub>2</sub>/C<sub>f,L</sub>, AP- ZrB<sub>2</sub>/C<sub>f,T</sub>, respectively.

<sup>\*</sup>corresponding author, e-mail: pietro.galizia@istec.cnr.it

Journal of the European Ceramic Society Volume 40, Issue 7, July 2020, Pages 2691-2698

2.2. Dilatometric analysis

For thermal damage determination, 5 consecutive cycles from low temperature (in the range

of 40-100°C) up to 1300°C were carried out using a horizontal dilatometer (Netzsch mod. DIL E

402, Germany), on 25 mm x 2.5 mm x 2 mm bars (Fig. 1a), under flowing argon of 100 ml/min,

 $10^{\circ}$ C/min heating rate. The relative dimensional change ( $\Delta$ L/L<sub>0</sub>) vs. temperature was recorded

both along TD (sample named TC-ZrB<sub>2</sub>/ $C_{f,T}$ ) and LD (sample named TC-ZrB<sub>2</sub>/ $C_{f,L}$ ) . The

coefficient of thermal expansion (CTE) was measured from the slope of the secant line joining

the values at 100°C and 1300°C. After 5 cycles, TD and LD bars were also indented as explained

below.

2.3. Indentation analysis

10 and 20 Kg indentations were introduced through a Micro Hardness Tester (Innovatest

Falcon 500, Netherlands) equipped with a standard Vickers diamond pyramid indenter, as

explained below.

a) In order to study the indentation damage, 3 Vickers indentations with a 10 kg load

were applied on 25x2.5 and 25x2 mm<sup>2</sup> surfaces (fiber's plane and out-of-fiber's plane,

respectively, see Fig. 1b) of both as produced composites (AP-ZrB<sub>2</sub>/C<sub>f,T</sub> and AP-ZrB<sub>2</sub>/C<sub>f,L</sub>,

respectively) and thermally cycled composites (TC-ZrB<sub>2</sub>/C<sub>f,T</sub> and TC-ZrB<sub>2</sub>/C<sub>f,L</sub>,

respectively). One of the diagonals of each of the indentations was aligned parallel to

the test specimen length. The indentations were characterized through SEM and

digital microscopy (HIROX RH 2000, Japan). From the obtained 3D reconstruction of

the imprints, the indentation profiles along the two diagonals were extrapolated.

b) A load of 20 kg was applied to 25x2.5 mm<sup>2</sup> tensile surface of AP-ZrB<sub>2</sub>/C<sub>f,T</sub> specimens

(Fig. 1c), which then were mechanically tested as described in the following (I-ZrB<sub>2</sub>/C<sub>f,T</sub>

specimens). We chose to apply an higher indentation load to I-ZrB<sub>2</sub>/C<sub>f,T</sub> specimens in

order to mechanically test the beams with a damage size as large as possible. The

indentation load of 20 kg was decreased down to 10 kg in order to avoid the break

under indentation of TC.

https://doi.org/10.1016/j.jeurceramsoc.2019.12.038

\*corresponding author, e-mail: pietro.galizia@istec.cnr.it

5

<u>Journal of the European Ceramic Society</u> <u>Volume 40, Issue 7, July 2020, Pages 2691-2698</u>

#### 2.4. Bending test

4-point flexural strength ( $\sigma$ ) was measured at room temperature according to ENV843–1:2006 standard for advanced ceramics. Specimens with dimensions of 25×2.5×2 mm<sup>3</sup> (length × width × thickness) were tested with a lower span of 20 mm and an upper span of 10 mm using a Zwick-Roell Z050 testing machine. The crosshead speed was fixed to 1 mm/min. Three bars for each kind of specimen were tested:

- as produced composite, labelled as AP-ZrB<sub>2</sub>/C<sub>f,T</sub>;
- thermally cycled composite with the above dilatometric analysis, labelled as TC-ZrB<sub>2</sub>/C<sub>f,T</sub>;
- indented composite, labelled as I-ZrB<sub>2</sub>/C<sub>f,T</sub>.

T subscript means that all the bars were tested with the fiber aligned transversally to the tensile stress, as shown in the sketch (Fig. 1c). It worth noticing that specimen geometry and bending test configuration were chosen in order to avoid the shear failure, and to ensure that fracture occurs in a tensile mode, i.e. transverse tensile failure. The conditions were identified through a comparison of the maximum values of tensile ( $\sigma_t$ ) and shear ( $\tau_i$ ) stress achieved during the bending test and the critical values of these stresses needed to initiate tensile and shear failure,  $\sigma_{t,c} = 63 \pm 7$  MPa and  $\tau_{i,c} = 36 \pm 4$  MPa, respectively [1]. The resulting condition to avoid the shear failure is:

$$\frac{\tau_{i,c}}{\sigma_{t,c}} > \frac{t}{s} \tag{1}$$

Hence the present conditions:  $\tau_{i,c}/\sigma_{t,c}$  and t/s = 2/20 (thickness-to-lower span ratio), widely satisfy the Eq.(1), at least for the AP-ZrB<sub>2</sub>/C<sub>f,T</sub> bars.

https://doi.org/10.1016/j.jeurceramsoc.2019.12.038

<sup>\*</sup>corresponding author, e-mail: pietro.galizia@istec.cnr.it

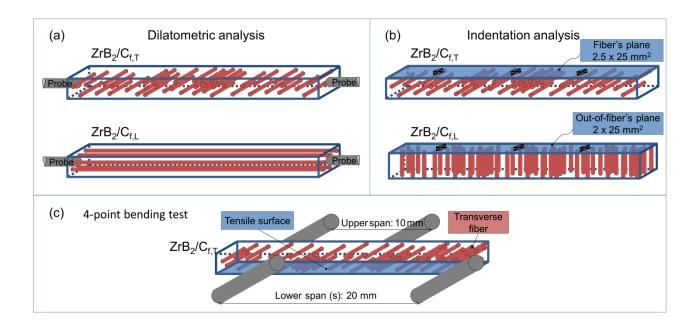


Fig. 1. Sketch of the composites configuration for the (a) dilatrometric analysis, where probes push the 2.5x2 mm<sup>2</sup> surfaces for both transversal and longitudinal fiber configurations:  $ZrB_2/C_{f,T}$ , and  $ZrB_2/C_{f,L}$ , respectively. (b) 10 kg Vickers indentation: 3 indentations were done on the 25x2.5 mm<sup>2</sup> surface (fiber's plane) or 25x2 mm<sup>2</sup> surface (out-of-fiber's plane) for  $ZrB_2/C_{f,T}$  and  $ZrB_2/C_{f,L}$ , respectively, and in both material states: as-produced (AP) and thermally cycled (TC). (c) 4-point bending test was performed in the transversal configuration for AP, TC and 20 kg Vickers indented specimens. All the beams with dimensions of 25×2.5×2 mm<sup>3</sup> (length × width × thickness) were drawn with isometric cavalier perspective (angle between x- and z-axis is 150° for (a) and (b), and 255° for (c)).

#### 3. Results and discussion

#### 3.1. Microstructure

Figure 2 shows the typical interface between matrix and fiber. Both in the transverse cross section (Figs. 2a,b) and in longitudinal cross section (Figs. 2c,d), the fiber/matrix interface was jagged suggesting a mechanical interlocking phenomenon. The degree of interlocking (e.g. the degree of warping) was affected by the matrix shrinkage during densification and was allowed by both the anisotropic microstructure of the carbon fibers and the presence of voids between the graphene layers [13]. We speculate that during densification the matrix compressed the fibers that plastically deformed allowing the penetration of ZrB<sub>2</sub> grains and the formation of

<sup>\*</sup>corresponding author, e-mail: pietro.galizia@istec.cnr.it

# <u>Journal of the European Ceramic Society</u> <u>Volume 40, Issue 7, July 2020, Pages 2691-2698</u>

jagged interfaces [20]. This interface configuration was very efficient in terms of stress transfer between matrix and fiber and did not hinder the fiber pull-out [13]. In fact, since the van der Waals bonding between the graphene layers in pitch-derived  $C_f$  is considerably weak, the interface debonding did not occur between the fiber and the matrix, but between inner graphene layers [13]. On the other hand, the strong fiber/matrix interface allowed the stress build-up during the cooling step of the sintering and left the material in a stressed state after sintering with homogeneously spaced cracks in the matrix (periodicity of 25  $\pm 10 \,\mu m$ , Fig. 2c). Similar observations were reported and discussed more in detail in a previous work [20]. In correspondence of the cracks both matrix and fiber released their residual stress and for that, in the following, this portion of fiber was defined as "inner freed fiber" (IFF).

<sup>\*</sup>corresponding author, e-mail: pietro.galizia@istec.cnr.it

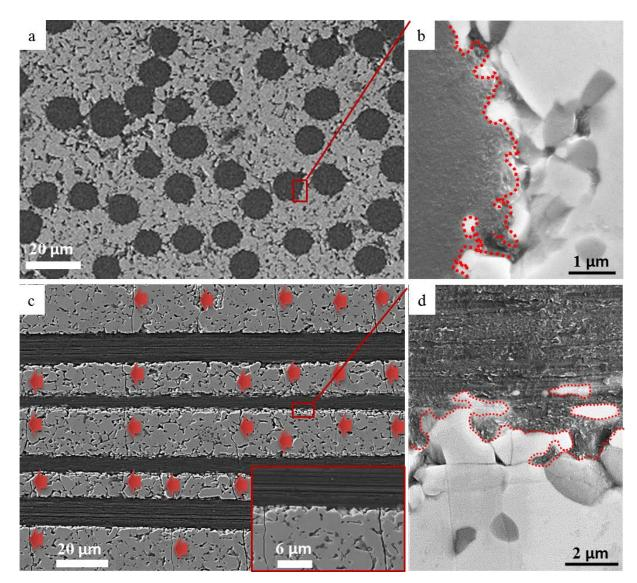


Fig. 2. SEM micrographs of the polished cross section of the UHTCMC based on pitch-derived carbon fibers and  $ZrB_2/SiC$  matrix along (a,b) the transverse direction, and (c,d) longitudinal direction. The dotted lines highlight the jagged fiber/matrix interface. The arrows point the presence of cracks in the matrix. The inset in © shows a detail of the cracked matrix.

#### 3.2. Thermal damage

Experimental curves in Fig. 3 show the relative dimensional change ( $\Delta L/L_0$ ) versus temperature up to 1300°C for polycrystalline  $ZrB_2$  [21], typical anisotropic pitch-derived carbon fibers along their transverse ( $C_{f,T}$ ) and longitudinal ( $C_{f,L}$ ) direction [22], and unidirectional  $C_{f}$ -reinforced  $ZrB_2$ -matrix of this work along the transverse ( $ZrB_2/C_{f,T}$ ) and longitudinal ( $ZrB_2/C_{f,L}$ ) direction. All the

<sup>\*</sup>corresponding author, e-mail: pietro.galizia@istec.cnr.it

above curves were fitted with polynomial equations and the coefficients were reported in Table 1. As expected,  $\Delta L/L_0$  of the composites along TD and of polycrystalline ZrB<sub>2</sub> were very close to each other and also very comparable with that of  $C_{f,T}$  (Fig. 3a). In fact, the obtained CTE of ZrB<sub>2</sub>/C<sub>f,T</sub> was intermediate between that of fiber and matrix (Table 1). The overlapping of  $\Delta L/L_0$  of the composite with that of the matrix and its deviation from that of the fiber may be ascribed to the easy interlayer graphene sliding which was allowed by the weak van der Waals force interaction [23,24]. In fact, C<sub>f</sub> could be easily deformed along the radial axis by untangling and restacking of the graphene sheets within the macroscopic fiber structure [25,26]. This reassembly of graphene sheets avoided their elastic shrinkage along the longitudinal axis – e.g. the solicitation of strong sp<sup>2</sup> bond – and allowed fibers to plastically deform and easily follow the different dilation of the matrix along TD, where CTE mismatch between matrix and fiber was -3.6·10<sup>-7</sup> °C<sup>-1</sup>. From Fig. 3b it can be seen that this small CTE mismatch and the supposed facile plastic deformation of the fiber along TD did not affect the overall CTE of the composites with the succession of thermal cycles. In fact,  $\Delta L/L_0$  loops were almost overlapped, and CTE of the composite, at the end of thermal cycling, decreased of just 0.9 % (Table 1). On the contrary, the large linear CTE mismatch of  $+7.3 \cdot 10^{-6} \, ^{\circ}\text{C}^{-1}$  between matrix and fiber along LD (Fig. 3c) led to a decrease of 52 % of the longitudinal CTE (from 1.75·10<sup>-6</sup> °C<sup>-1</sup> to 0.84·10<sup>-6</sup> °C<sup>-1</sup>, Table 1), and a permanent expansion of 0.47 % at RT (Fig. 3d). The absolute value of the permanent expansion corresponded to about 120 µm. We hypothesized that this value could be correlated to the matrix cracking which led to the matrix shrinkage (releasing of tensile stresses) and fiber elongation (releasing of compressive stresses) along LD. Hence, this releasing of elastic strain led to the formation of IFF.

<sup>\*</sup>corresponding author, e-mail: pietro.galizia@istec.cnr.it

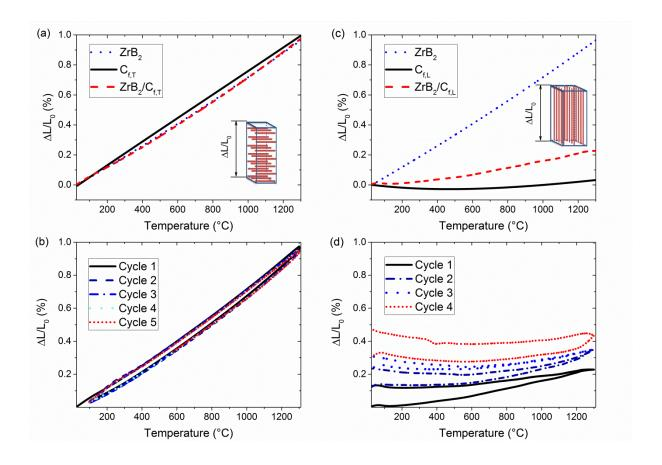


Fig. 3. (a) Relative dimensional change ( $\Delta L/L_0$ ) vs. temperature (T) of tested UHTCMC ( $ZrB_2/C_{f,T}$ , dashed line) along the transversal direction together with that of polycrystalline  $ZrB_2$  [21] (dotted line), and pitch-derived fibers [22] ( $C_{f,T}$ , solid line) along the transversal direction. (b) Measured dilatometry curves of  $ZrB_2/C_{f,T}$  during thermal cycles. (c)  $\Delta L/L_0$  vs. T of tested UHTCMC ( $ZrB_2/C_{f,L}$  dashed line) along the longitudinal direction together with that of polycrystalline  $ZrB_2$  [21] (dotted line), and pitch-derived fibers [22] ( $C_{f,L}$  solid line) along the longitudinal direction. (b) Measured dilatometry curves of  $ZrB_2/C_{f,L}$  during thermal cycles.

<sup>\*</sup>corresponding author, e-mail: pietro.galizia@istec.cnr.it

**Table 1** Cycles number (#). Polynomial coefficients of measured relative dimensional change  $(\Delta L/L_0)$ :  $a_4$ ,  $a_3$ ,  $a_2$ ,  $a_1$ , and  $a_0$ . Secant CTE in selected temperature range of 100-1300°C.

Materials	#	a <sub>4</sub>	<b>a</b> <sub>3</sub>	a <sub>2</sub>	a <sub>1</sub>	$a_0$	CTE	Ref.
		(°C <sup>-4</sup> )	(°C <sup>-3</sup> )	(°C <sup>-2</sup> )	(°C <sup>-1</sup> )		(10 <sup>-6</sup>	
							°C <sup>-1</sup> )	
ZrB <sub>2</sub>	1	_	_	6.65193E-	6.69346E-	-1.7922E-	7.51	_
				10	6	4		
$C_{f,T}$	1	_	1.238E-13	-2.87108E-	8.03756E-	-2.8383E-	7.87	[22]
				10	6	4		
$C_{f,L}$	1	1.152E-16	-7.35902E-	2.11178E-	-	4.56636E-	0.25	[22]
			13	9	1.54005E-	5		
					6			
$ZrB_2/C_{f,T}$	1	-2.37084E-	6.0085E-	-4.10573E-	8.0073E-6	6.39353E-	7.70	-
		15	12	9		5		
$ZrB_2/C_{f,T}$	5	-2.45087E-	5.94493E-	-3.73478E-	7.70884E-	5.25088E-	7.63	-
		15	12	9	6	5		
$ZrB_2/C_{f,L}$	1	6.55164E-	-1.91583E-	3.52715E-	-	1.04914E-	1.75	-
		16	12	9	5.23633E-	4		
					7			
$ZrB_2/C_{f,L}$	4	4.05192E-	-3.70271E-	4.44807E-	-	3.16065E-	0.84	_
		16	12	9	2.58827E-	4		
					6			

#### 3.3. Indentation damage

In order to study the indentation damage, 10 kg Vickers imprints were made on the fiber's plane (first column of Fig. 4) and out-of-fiber's plane (second column of Fig. 4) of both as produced (AP, Figs. 4a,b) and thermally cycled (TC, Figs. 4c,d) specimens.

# 3.3.1. Indentation onto the fiber's plane

After indentation in the fiber's plane (Figs. 4a,c), material pile-up was observed. Indeed, during loading, fibers were forced to bend until they broke and released their compression state,

<sup>\*</sup>corresponding author, e-mail: pietro.galizia@istec.cnr.it

producing a widespread pile-up. The pile-up height of as produced (AP) specimens was higher than that of thermally cycled (TC) specimens (Fig. 4e). This result is in agreement with the expected initial residual stress level. In fact, since TC specimens should have released their residual stress by matrix cracking and consequent formation of IFFs, the swelling of AP samples resulted bigger. The pile-up term, reminiscence of metal work hardening, should be intended as spring up of material outside the surface since the material inside is constrained. The pile-up propagation across the surface was larger in TD, where the elastic modulus of the composite, Ec.T, is smaller (70 GPa), on the other hand it is smaller in LD where Ec.L is higher (230 GPa). Looking beneath the initial surface – at the imprints left by the tip – the indentation depth (h) and diagonal (d) of TC samples are about 37 % deeper and 25 % larger those that of AP samples (Table 2). These differences are significant and match the significant decreasing of matrix modulus with thermal cycles, which has been estimated to decrease from ≈200 GPa to few tens of GPa after three thermal cycles up to 1300°C [20]. Hence, on the fiber's plane the thermal cycles decreased the material stiffness as well as its hardness. The lower d/h value (r) of both AP, and TC with respect to the theoretical one and to the experimental one measured on the monolithic ZrB<sub>2</sub>-based ceramic [27] was due to the higher elastic spring back of C<sub>f</sub> along the x-axis with respect to that along z-axis (Table 2). In other words, the elastic spring back of the fibers, dispersed within the matrix, showed the tendency to close the imprint. The higher spring back of TC specimens with respect to AP ones ( $r_{TC-ZrB_2/C_{f,T}} < r_{AP-ZrB_2/C_{f,T'}}$  Table 2) could be due to the higher amount of IFF. r <sub>ZrB</sub>, of 9.8 is in agreement with the value that can be extrapolated from the Berkovich nanoindentation on ZrB<sub>2</sub> ceramic grains by Csanadi et al. [28]. In fact, considering that Berkovich indenter gives the same projected area-to-depth ratio as the Vickers indenter and that the projected areas of loaded and unloaded imprint are the same, the  $h/h_{max}$  ratio of 0.62 corresponds to a  $r_{ZrB_2}$  of 11.3 [28,29]. The higher value extrapolated from the nanoindentation (11.3 > 9.8) could be ascribed to a more elastic response of the single ZrB<sub>2</sub> grain with respect to that of polycrystalline area, which could improve the plastic deformation. In Fig. 4e the theoretical Vickers imprints is drawn with the same depth of experimental ones in order (i) to better visualize the xy shrinkage of the experimental imprints, and (ii) to resume the parallelism with the pile-up of the metals, which is large only when  $h = h_{max}$  [30].

<sup>\*</sup>corresponding author, e-mail: pietro.galizia@istec.cnr.it

#### 3.3.2. Indentation onto the out-of-fiber's plane

From the characteristics of imprints into the out-of-fiber's plane (Table 2), it can be noted that r-values are higher than 7. This reverse result, with respect to that obtained into fiber's plane, was due to the C<sub>f</sub> spring back which this time acted along the z-axis. Also on the out-of-fiber's plane, as for fiber's plane, the spring back was bigger for the TC specimens ( $r_{TC-ZrB_2/C_{f_1}} > r_{AP-}$  $z_{rB_2/C_f}$ ) owing to the higher amount of IFF. If we consider  $r_{z_{rB_2}}$  instead of  $r_{Th.}$ , we can note that  $r_{\text{AP-ZrB}_2/C_{\text{f,L}}} \text{ was smaller than this reference, while } r_{\text{TC-ZrB}_2/C_{\text{f,L}}} \text{ was larger. } r_{\text{AP-ZrB}_2/C_{\text{f,L}}} < r_{\text{ZrB}_2} \text{ could be}$ ascribed to the damage induced by the indenter in the stressed AP specimens.  $r_{TC-ZrB_{\gamma}/C_{f_1}} >$  $r_{ZrB_2}$  can be justified considering that the IFFs can be easily buckled under the loading, hence permitted a deeper penetration, and then released a larger spring back. In Fig. 4f, it can be seen that the unloaded profile of TC specimen had a flatter shape and almost lost that of the Vickers' indenter. As for the AP specimen the induced damages may free some fibers from the matrix clamping. As consequence we found the appearance of fibers outside the area of imprint (out-of-plane freed fibers, OFF) visible in Figs. 4b,f. This phenomenon can be described as a sort of "button effect" or "antipull-out", since occurs by pushing in. To better characterize the indentation profiles on the out-of-fiber's plane, 5 cycles of loading-unloading indentation were performed. In this way, the elastic recovery of both IFF and OFF was suppressed by destroying the free fibers (Fig. 4f) and the calculated r-values match that of monolithic ZrB<sub>2</sub>.

<sup>\*</sup>corresponding author, e-mail: pietro.galizia@istec.cnr.it

**Table 2** Vickers indentation results: permanent depth (h) and diagonals (d) beneath the fiber's plane  $(ZrB_2/C_{f,T})$  and out-of-fiber's plane  $(ZrB_2/C_{f,L})$  in as-produced (AP) and thermally cycled (TC) composites, and monolithic  $ZrB_2$ .

Materials	Load	h	d	r = d/h
	(kg)	(µm)	(µm)	
AP-ZrB <sub>2</sub> /C <sub>f,T</sub>	10	30 ± 5	156 ± 6	5.2
$AP-ZrB_2/C_{f,L}$	10	24 ± 1	207 ± 17	8.6
AP-ZrB <sub>2</sub> /C <sub>f,L</sub> (reloaded x5)	10	24 ± 1	235 ± 8	9.9
$TC-ZrB_2/C_{f,T}$	10	41 ± 4	195 ± 21	4.8
$TC-ZrB_2/C_{f,L}$	10	24 ± 3	311 ± 12	13
$TC-ZrB_2/C_{f,L}$ (reloaded x5)	10	41 ± 2	356 ± 14	9
Monolithic ZrB <sub>2</sub>	1	2.9 ± 0	28.3 ± 1.1	9.8
Theoretical Vickers imprint	-	1	7	7

<sup>\*</sup>corresponding author, e-mail: pietro.galizia@istec.cnr.it

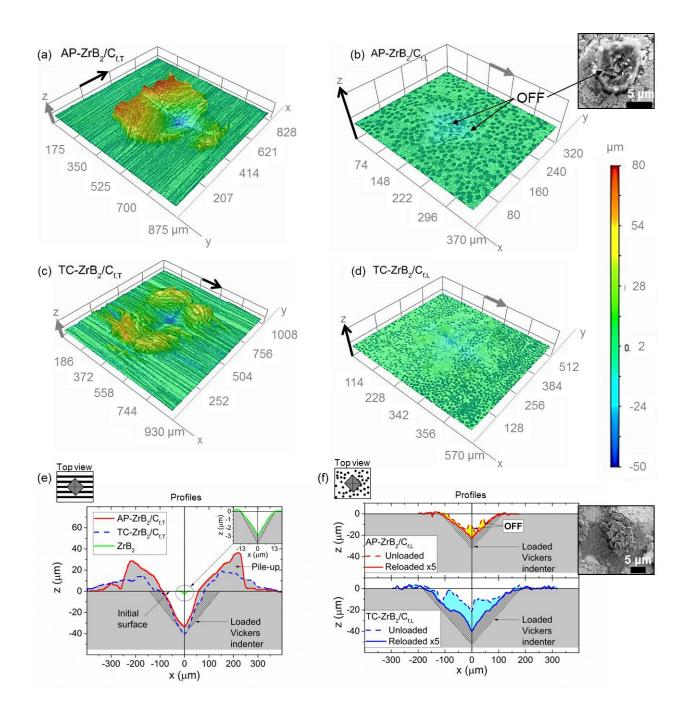


Fig. 4. 3D colored map of as-produced, AP, (a,b) and thermally cycled, TC, (c,d) specimens indented onto fiber's plane (first column) and out-of-fiber's plane (second column). The gray and black arrows indicate the stacking direction of the unidirectional fabrics, and the longitudinal direction of the fibers, respectively. Red and blue colors indicate the higher and the lower height, respectively. The four 3D maps have the same z-scale and the initial surfaces are at the same level:  $z \approx 0 \mu m$ . (b-inset) SEM of out-of-plane fibers (OFF). (e) Typical profile of the

<sup>\*</sup>corresponding author, e-mail: pietro.galizia@istec.cnr.it

diagonal impression made on fiber's plane of AP (red solid line) and TC specimens (blue dashed line), and monolithic  $ZrB_2$ -based ceramic (black solid area close to the origin axes). (f) Typical profiles of the indenter's diagonal made on out-of-fiber's plane of AP (dashed line in the upper plot) and TC specimens (dashed line in the lower plot), and after five load-unload cycles (solid lines). In all the profile plots, the horizontal axis intercepting y = 0 and represents the initial surface. The areas filled with lines pattern represents the theoretical profile of the Vickers indenter at the maximum load of 10 kg. (f-inset) SEM of out-of-plane fibers (OFF) after five loading-unloading cycles. (For interpretation of the references to colour in this figure legend, the reader is referred to the Web version of this article.)

#### 3.4. Retained fracture strength after thermal cycling

After thermal cycling from RT to 1300°C for 5 times, the retained strength was measured and compared to the pristine one (Fig. 5a). Despite the damage introduced by thermal treatments decreased the matrix elastic modulus as shown in earlier studies [20], the strength did not undergo appreciable variation, starting from 63 ±7 MPa and remaining 62 ± 24 MPa. Generally, when monolithic ceramics are subjected to a thermal damage, they show a retained average strength lower than 30 % of the pristine value, and an increase of data dispersion [31,32]. In our case, since the orientation angle of fibers to the tensile direction is 90°, specimens were tested in matrix-dominated loading configuration where  $C_f$  acted more as long defective channels, rather than reinforcing phase. Hence, both AP and TC  $ZrB_2/C_{f,T}$  samples can be considered as bulk  $ZrB_2$  materials affected by a 45 % of anisotropic porous channels. This observation leads to justify the obtained  $\sigma$  values which are similar to that of other porous ceramics with similar architecture [33]. The reason of the higher  $\sigma$  values and damage tolerance with respect to the correspondent isotropic porous ceramics is generally ascribed to the higher tensile strength of the larger struts, and to the crack tip blunting due to the circular shape of fibers section [33,34].

Moreover, these results give a different perspective to the concept of damage tolerance. In fact, if along the longitudinal direction it was mainly the matrix porosity that enabled the damage tolerance by reducing the interlaminar shear strength (generally below 20 MPa) as a consequence of the lower matrix and matrix/fiber interface strengths [35,36], along the transverse direction it is the inverse: fibers, acting as pores, enabled the damage tolerance of

<sup>\*</sup>corresponding author, e-mail: pietro.galizia@istec.cnr.it

the dense matrix characterized by strong fiber/matrix interfaces. In the context of off-axis composite strength and damage tolerance, such aging treatment was not detrimental, as well as the high matrix density and the strong interfaces. In other words, this work suggests that neither high temperature cycling nor high matrix density and strong interface were detrimental for off-axis strength and damage tolerance.

Looking at the fracture surface of AP specimen (Figs. 5b,c), it can be seen that failure occurred mainly through the matrix and was accompanied by delamination between orthogonal unidirectional fabrics and fiber "scissoring", but with minimal fiber fracture. Fiber scissoring was maximized when the fracture occurred in the plane orthogonal to the unidirectional fabrics and transversal to the fiber axis (Fig. 5b). In this surface, crack tip blunting was clearly visible. The same toughening mechanism was observed for TC specimens (not shown ). This observation supports what is surmised above: in both cases (AP and TC) the off-axis damage tolerant behaviour was not yielded by the fibers in itself, but should be ascribed to the blunting effect produced by the "channels" produced by the fibers. The fracture surface of TC specimen (Fig.5 d) displayed a combination of fiber "scissoring" and "ripping". Furthermore, its matrix cracks appeared wider than that of AP specimen. These observations suggest a to lower efficacy of the TC matrix, with respect to the AP matrix, in intensifying stress concentrations around fiber breaks. Anyway in both cases interlaminar shear failure was not observed (i.e. H-crack formation), in agreement with the designed failure (Eq. (1)), and the expected matrix-dominated loading behaviour guaranteed by the dense-matrix.

#### 3.5. Retained fracture strength after Vickers indentation

Through Vickers indentation of 20 kg, a damage of 50  $\mu$ m depth was introduced. The damaged specimens (labeled with I) showed a the fracture strength of, 84  $\pm$  20 MPa, e.g. higher than that of AP specimens (63  $\pm$  7 MPa). This feature was somewhat misleading in the sense that fracture did not started from the flaw, but quite far ( $\approx$ 1 mm) from that, and hence the indentation did not act as critical defect. Hence, the composite displayed a damage insensitivity [37]. The reason for this unexpected result could be the releasing of tensile stress of the matrix and the consecutive strengthening of the volume involved by the process zone (estimated to be  $\approx$  1 mm³). Thus, the volume from which fracture-initiation took place should be reduced of about 20 %. This value, all approximations aside, was a relevant part and not a

<sup>\*</sup>corresponding author, e-mail: pietro.galizia@istec.cnr.it

fraction, and, according to the Weibull statistics, can justify the apparent increase of the fracture strength and the broadening of the dispersion.

For sake of comparison in Fig. 5, the stress-displacement curve of a typical monolithic ZrB<sub>2</sub> + 10 vol% SiC [27] is shown together with that obtained after 2 kg indentation (5 μm depth) [38]. The monolithic ceramic retained about 24 % of the pristine strength (from  $637 \pm 80$  MPa to 156 ± 11 MPa) [27,38]. The strength retention improved when ceramics were reinforced. For example, by reinforcing Al<sub>2</sub>O<sub>3</sub> with 30 vol% SiC whisker instead of nano-sized SiC particles, the retained strength, after a Vickers imprint of about 50 μm depth, increased from 48 % to 72 %. In any case, the observed notch insensitivity is particularly striking: the fibers aligned along TD could not bridge the crack walls and the strength drop should be comparable with that of the particulate composite [39], instead of remaining unchanged. The reason could be that neither the transverse dimension of the fibres (10  $\mu$ m) nor the indentation damage (50  $\mu$ m) represented the critical flaw size, but the latter could consist in multiple transverse fiber sections linked by matrix cracking (> 50 μm). This explanation is not fully convincing since, contrary to the result presented in 3.4 section, the critical flaw size and/or density should increase with the thermal damage and decrease the transverse strength. Anyway, the retention of the off-axis strength after thermal damaging or indentation suggests that not only UHTCMCs can bear thermal cycles, thermal gradient, vibrations, debris impacts, etc. but also, if we look to the ratio of transverse to longitudinal strengths,  $\sigma_T / \sigma_L = 0.18$  ( $\sigma_T = 65$  MPa,  $\sigma_L = 360$ MPa), that carbon fiber-reinforced dense UHTCs can bear the transverse load without need cross-ply architecture. In fact, this baseline UHTCMCs showed a transverse strength and strength isotropy more than three times higher than that of conventional non-woven CMCs ( $\sigma_T$ = 3-20 MPa,  $\sigma_T/\sigma_L$  = 0.004-0.029 MPa, respectively [40-42]).

<sup>\*</sup>corresponding author, e-mail: pietro.galizia@istec.cnr.it

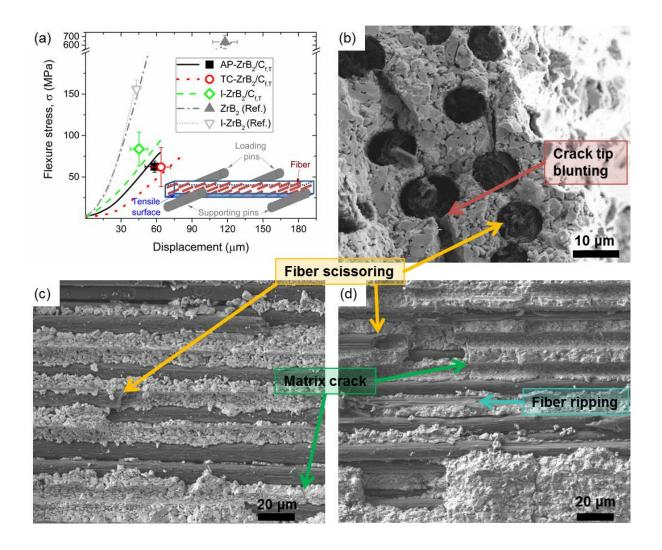


Fig. 5. (a) Typical flexure stress vs. crosshead displacement curves obtained with a 4-point bending test for the as produced specimens ( $AP-ZrB_2/C_{f,T}$ : solid line, and monolithic  $ZrB_2$  [27]: dash-dotted line), thermally cycled specimens ( $TC-ZrB_2/C_{f,T}$ , dotted line), intended specimens on the tensile surface ( $I-ZrB_2/C_{f,T}$ : dashed line, indented monolithic  $I-ZrB_2$  [38]: short dotted line). The symbols (solid square for  $AP-ZrB_2/C_{f,T}$ , open circle for  $TC-ZrB_2/C_{f,T}$ , open diamond for  $I-ZrB_2/C_{f,T}$ , solid up triangle for  $ZrB_2$ , and open down triangle for  $I-ZrB_2$  [38]) represent the mean values of the fracture strength at breaking displacement. SEM of fracture surfaces along (b) the thickness-for-length surface and (c) thickness-for-width surfaces of as produced specimen, and (d) along thickness-for-width surfaces of thermally cycled specimen. An example of crack tip blunting, fiber scissoring, fiber ripping, and matrix crack is pointed by an arrow in each electron micrograph.

<sup>\*</sup>corresponding author, e-mail: pietro.galizia@istec.cnr.it

#### **4 Conclusions**

The off-axis strength retention of ultra-high temperature ceramic matrix composites (UHTCMCs) based on ZrB2-matrix reinforced with 45 vol% of unidirectional continuous carbon fibers was investigated after inducing thermal or indentation damage. The results proved that UHTCMCs kept their load bearing capability in both cases, and showed damage insensitivity although tested in fully matrix-dominated loading configuration (off-axis configuration). The retention of off-axis properties after thermal damaging or indentation suggested that UHTCMCs can bear thermal cycles, thermal gradient, vibrations, debris impacts, etc., and can really lead to a breakthrough in the aerospace field. Furthermore, thermal damage accumulation and decrease of residual stresses did not affect the coefficient of thermal expansion along the transverse direction. On the other side, thermal damage led i) to a deeper imprint, and ii) to a larger elastic recovery owing to the larger amount of inner freed fiber.

#### **Acknowledgments**

The research leading to these results has received funding from the European Union's Horizon 2020 research and innovation programme under grant agreement C3HARME No. 685594. The authors are grateful to A.N. Murri for thermal dilatometric measurements.

#### References

[1] L. Zoli, A. Vinci, P. Galizia, C. Melandri, D. Sciti, On the thermal shock resistance and mechanical properties of novel unidirectional UHTCMCs for extreme environments, Sci. Rep. 8 (2018) 9148. https://doi.org/10.1038/s41598-018-27328-x

[2] N.P. Padture, Advanced structural ceramics in aerospace propulsion, Nat. Mater. 15 (2016) 804–809. https://doi.org/10.1038/nmat4687

[3] D. Sciti, L. Zoli, L. Silvestroni, A. Cecere, G.D. Di Martino, R. Savino, Design, fabrication and high velocity oxy-fuel torch tests of a  $C_{f^-}ZrB_{2^-}$  fiber nozzle to evaluate its potential in rocket motors, Mater. Des. 109 (2016) 709–717. https://doi.org/10.1016/j.matdes.2016.07.090

[4] S. Vorotilo, K. Sidnov, I. Yu. Mosyagin, A.V. Khvan, E.A. Levashov, E.I. Patsera, I.A. Abrikosov, Ab-initio modeling and experimental investigation of properties of ultra-high temperature

<sup>\*</sup>corresponding author, e-mail: pietro.galizia@istec.cnr.it

- solid solutions  $Ta_xZr_{1-x}C$ , J. All. Comp. 778 (2019) 480-486. https://doi.org/10.1016/j.jallcom.2018.11.219
- [5] J. Zou, H.-B. Ma, L. Chen, Y.-J. Wang, G.-J. Zhang, Key issues on the reactive sintering of  $ZrB_2$  ceramics from elementary raw materials; Scr. Mater. 164 (2019) 105–109. https://doi.org/10.1016/j.scriptamat.2019.01.044
- [6] E.P. Simonenko, N. P. Simonenko, A. N. Gordeev, A. F. Kolesnikov, V. G. Sevastyanov, N. T. Kuznetsov, Behavior of HfB<sub>2</sub>–30 vol% SiC UHTC obtained by sol–gel approach in the supersonic airflow, J. Sol-Gel Sci. Technol. (2019). https://doi.org/10.1007/s10971-019-05029-9
- [7] K. Kavakeb, Z. Balak, H. Kafashan, Densification and flexural strength of  $ZrB_2$ –30 vol% SiC with different amount of  $HfB_2$ , Int. J. Refract. Met. H. 83 (2019) 104971. https://doi.org/10.1016/j.ijrmhm.2019.104971
- [8] S. Karimirad, Z. Balak, Characteristics of spark plasma sintered ZrB<sub>2</sub>-SiC-SCFs composites, Ceram. Int. 45 (2019) 6275–6281. https://doi.org/10.1016/j.ceramint.2018.12.109
- [9] S. Failla, P. Galizia, L. Zoli, A. Vinci, D. Sciti, Toughening effect of non-periodic fiber distribution on crack propagation energy of UHTC composite, J. All. Comp. 777 (2018) 612-618. https://doi.org/10.1016/j.jallcom.2018.11.043
- [10] P. Hu, D. Zhang, S. Dong, Q. Qu, X. Zhang, A novel vibration-assisted slurry impregnation to fabricate  $C_f/ZrB_2$ -SiC composite with enhanced mechanical properties, J. Eur. Ceram. Soc. 39 (2018) 798-805. https://doi.org/10.1016/j.jeurceramsoc.2018.10.029
- [11] D. Zhang, P. Hu, S. Dong, Q. Qu, X. Zhang, Effect of pyrolytic carbon coating on the microstructure and fracture behavior of the  $C_f/ZrB_2$ -SiC composite, Ceram. Int. 44 (2018) 19612-19618. https://doi.org/10.1016/j.ceramint.2018.07.210
- [12] C. Fang, P. Hu, S. Dong, P. Xie, K. Wang, X. Zhang, Design and optimization of the coating fibers and sintering temperature for  $ZrB_2$ -SiC-C<sub>f</sub> composites prepared by hot pressing, J Eur. Ceram. Soc 39 (2019) 2805-2811. https://doi.org/10.1016/j.jeurceramsoc.2019.03.038
- [13] P. Galizia, S. Failla, L. Zoli, D. Sciti, Tough salami-inspired  $C_f/ZrB_2$  UHTCMCs produced by electrophoretic deposition, J. Eur. Ceram. Soc. 38 (2018) 403–409. https://doi.org/10.1016/j.jeurceramsoc.2017.09.047
- [14] H. Hu, Q. Wang, Z. Chen, C. Zhang, Y. Zhang, J. Wang, Preparation and characterization of C/SiC–ZrB<sub>2</sub> composites by precursor infiltration and pyrolysis process, Ceram. Int. 36 (2010) 1011–1016. https://doi.org/10.1016/j.ceramint.2009.11.015

<sup>\*</sup>corresponding author, e-mail: pietro.galizia@istec.cnr.it

- [15] W.-C. Tu, F.F. Lange, A.G. Evans, Concept for a damage-tolerant ceramic composite with "strong" interfaces, J. Am. Ceram. Soc. 79:2 (1996) 417-24. https://doi.org/10.1111/j.1151-2916.1996.tb08138.x
- [16] E.A.V. Carelli, Effects of thermal aging on the mechanical properties of a porous-matrix ceramic composite, J. Am. Ceram. Soc. 85:3 (2002) 595-602. https://doi.org/10.1111/j.1151-2916.2002.tb00138.x
- [17] G.-J. Zhang, J.-F. Yang, T. Ohji, Fabrication of porous ceramics with unidirectionally aligned continuous pores, J. Am. Ceram. Soc. 84:6 (2001) 1395-1397. https://doi.org/10.1111/j.1151-2916.2001.tb00849.x
- [18] J.A. Heathcote, X.-Y. Gong, J.Y. Yang, U. Ramamurty, F.W. Zok, In-plane mechanical properties of an all-oxide ceramic composite, J. Am. Ceram. Soc. 82 [10] (1999) 2721-30. https://doi.org/10.1111/j.1151-2916.1999.tb02148.x
- [19] F.W. Zok, C.G. Levi, Mechanical properties of porous-matrix ceramic composites, Adv. Eng. Mater. 3 (2001) 15-23. https://doi.org/10.1002/1527-2648(200101)3:1/2<15::AID-ADEM15>3.0.CO;2-A
- [20] P. Galizia, L. Zoli, D. Sciti, Impact of residual stress on thermal damage accumulation, and Young's modulus of fiber-reinforced ultra-high temperature ceramics, Mater. Des. 160 (2018) 803-809. https://doi.org/10.1016/j.matdes.2018.10.019
- [21] F. Monteverde, S. Guicciardi, A. Bellosi, Advances in microstructure and mechanical properties of zirconium diboride based ceramics, Mater. Sci. Eng. A 346 (2003) 310–319. https://doi.org/10.1016/S0921-5093(02)00520-8
- [22] C. Pradere, C. Sauder, Transverse and longitudinal coefficient of thermal expansion of carbon fibers at high temperatures (300–2500 K), Carbon 46 (2008) 1874–1884. https://doi.org/10.1016/j.carbon.2008.07.035
- [23] W. Wang, S. Dai, X. Li, J. Yang, D. J. Srolovitz, Q. Zheng, Measurement of the cleavage energy of graphite, Nat. Commun. 6 (2015) 7853. https://doi.org/10.1038/ncomms8853
- [24] G. Xin, T. Yao, H. Sun, S. M. Scott, D. Shao, G. Wang, J. Lian, Highly thermally conductive and mechanically strong graphene fibers, Science 349 (2015) 1083-1087.

https://doi.org/10.1126/science.aaa6502

<sup>\*</sup>corresponding author, e-mail: pietro.galizia@istec.cnr.it

- [25] Z. Xu, Y. Liu, X. Zhao, L. Peng, H. Sun, Y. Xu, X. Ren, C. Jin, P. Xu, M. Wang, C. Gao, Ultrastiff and strong fraphene fibers via full-scale synergetic defect engineering, Adv.Mater. 28 (2016) 6449–6456. https://doi.org/10.1002/adma.201506426
- [26] G. Xin, W. Zhu, Y. Deng, J. Cheng, L. T. Zhang, A. J. Chung, S. De, J. Lian, Microfluidics-enabled orientation and microstructure control of macroscopic graphene fibres, Nature Nanotechnology 14(2919) 168–175. https://doi.org/10.1038/s41565-018-0330-9
- [27] F. Monteverde, S. Guicciardi, C. Melandri, D. Dalle fabbriche, Densification, Microstructure Evolution and Mechanical Properties of Ultrafine SiC Particle-Dispersed ZrB<sub>2</sub> Matrix Composites. In: Orlovskaya N., Lugovy M. (Eds.), Boron Rich Solids, NATO Science for Peace and Security Series B: Physics and Biophysics. Springer, Dordrecht, 2010, pp. 261-272. https://doi.org/10.1007/978-90-481-9818-4\_17
- [28] T. Csanádi, A. Kovalčíková, J. Dusza, W.G. Fahrenholtz, G.E. Hilmas, Slip activation controlled nanohardness anisotropy of ZrB<sub>2</sub> ceramic grains, Acta Mater. 140 (2017) 452-464. https://doi.org/10.1016/j.actamat.2017.08.061
- [29] W.C. Oliver, G.M. Pharr, Measurement of hardness and elastic modulus by instrumented indentation: advances in understanding and refinements to methodology, J. Mater. Res.19:1 (2004) 3-20. https://doi.org/10.1557/jmr.2004.19.1.3
- [30] E. Broitman, Indentation hardness measurements at macro-, micro-, and nanoscale: a critical overview, Tribol. Lett. 65:23 (2017) 1-18. https://doi.org/10.1007/s11249-016-0805-5
- [31] F. Monteverde, L. Scatteia, Resistance to thermal shock and to oxidation of metal diborides-SiC ceramics for aerospace application, J. Am. Ceram. Soc. 90, 1130–1138 (2007). https://doi.org/10.1111/j.1551-2916.2007.01589.x
- [32] W. Zhi, Q. Qiang, W. Zhanjun, S. Guodong, The thermal shock resistance of the ZrB<sub>2</sub>-SiC–ZrC ceramic, Mat. Des. 32 (2011) 3499–3503. https://doi.org/10.1016/j.matdes.2011.02.056
- [33] J. Cao, Z. Lu, K. Miao, H. Zhao, Y. Xia, F. Wang, B. Lu, Fabrication of high-strength porous SiC-based composites with unidirectional channels, J. Am. Ceram. Soc. (2019) 1–11. https://doi.org/10.1111/jace.16332
- [34] C. Tallon, C. Chuanuwatanakul, D.E. Dunstan, G.V Franks. Mechanical strength and damage tolerance of highly porous alumina ceramics produced from sintered particle stabilized foams, Ceram. Int. 42 (2016) 8478–8487. https://doi.org/10.1016/j.ceramint.2016.02.069

<sup>\*</sup>corresponding author, e-mail: pietro.galizia@istec.cnr.it

- [35] M.A. Mattoni, J.Y. Yang, C.G. Levi, F.W. Zok, Effects of matrix porosity on the mechanical properties of a porous-matrix, all-oxide ceramic composites, J. Am. Ceram. Soc. 84:11 (2001) 2594-602. https://doi.org/10.1111/j.1151-2916.2001.tb01059.x
- [36] O. Ševeček, L. Bertolla, Z. Chlup, L. Řehořek, Z. Majer, P. Marcián, M. Kotoul, Modelling of cracking of the ceramic foam specimen with a central notch under the tensile load, Theor. Appl. Fract. Mec. 100 (2019) 242-250. https://doi.org/10.1016/j.tafmec.2019.01.024
- [37] F. Tavangarian, D. Hui, G. Li, Crack-healing in ceramics. Compos. Part B-Eng. 144 (2018) 56-87. https://doi.org/10.1016/j.compositesb.2018.02.025
- [38] F. Saraga, F. Monteverde, Self-healing ability of ultra high temperature ceramics, in: L. Silvestroni, C. Galassi, E. Di Bartolomeo, M. Dondi (Eds.), Proceedings of the first workshop for young ceramists, Novembre 26-27, 2018, Bologna, Italy. La Mandragora s.r.l.
- [39] T. Osada, N. Wataru, K. Takahashi, K. Ando, Self-crack-healing behavior in ceramic matrix composites, in I.M. Low (Eds.), Advances in Ceramic Matrix Composites, Woodhead Publishing Series in Composites Science and Engineering, 2014, pp. 410-441. https://doi.org/10.1016/B978-0-08-102166-8.00021-9
- [40] R. Bhatt, R Phillips, Laminate behavior for SiC fiber-reinforced reaction-bonded silicon nitride matrix composites, J. Comps. Technol. Res. 12: 1 (1990) 13-23. https://doi.org/10.1520/CTR10173J
- [41] J. Koyanagi, H. Hatta, M. Kotani, H. Kawada, A comprehensive model for determining tensile strengths of various unidirectional composites, J. Compos. Mater. 43:18 (2009) 1901-1914. https://doi.org/10.1177/0021998309341847
- [42] D. Zhang, D.R. Hayhurst, Stress–strain and fracture behaviour of 0°/90° and plain weave ceramic matrix composites from tow multi-axial properties, Int. J. Solids Struct. 47 (2010) 2958-2969. https://doi.org/10.1016/j.ijsolstr.2010.06.023

https://doi.org/10.1016/j.jeurceramsoc.2019.12.038

<sup>\*</sup>corresponding author, e-mail: pietro.galizia@istec.cnr.it